Received 16 November 2021; revised 1 January 2022 and 19 January 2022; accepted 28 January 2022. Date of publication 7 February 2022; date of current version 4 March 2022. The review of this article was arranged by Editor Z. Zhang.

Digital Object Identifier 10.1109/JEDS.2022.3149381

Piston-Mode pMUT With Mass Load

LEI WANG [1] (Member, IEEE), JIE ZHOU [1] (Member, IEEE), WEI ZHU [1] (Member, IEEE), ZHIPENG WU [1], WENJUAN LIU [1,2] (Member, IEEE), AND CHENGLIANG SUN [1,2]

1 The Institute of Technological Sciences, Wuhan University, Wuhan 430072, China
2 Hubei Yangtze Memory Laboratories, Wuhan 430205, China

CORRESPONDING AUTHORS: W. LIU AND C. SUN (e-mail: lwjwhu@whu.edu.cn; sunc@whu.edu.cn)

This work was supported by the National Key Research and Development Program of China under Grant 2020YFB2008800.

ABSTRACT This paper proposes a novel piezoelectric micromachined ultrasonic transducer (pMUT) with a proof mass under the central circular diaphragm to enhance transmission efficiency and fractional bandwidth (FBW) in liquid-coupled operation. Compared with the traditional pMUT, the proposed pMUT has advantages: (1) the resonance frequency of pMUT can be adjusted by proof mass; (2) a large ratio of third-order resonance frequency to first-order resonance frequency can be obtained by an additional proof mass under the circular diaphragm; (3) the mode shape of proposed pMUT changes from Gaussian-like to piston-like, which enables higher transmission sensitivity; (4) the FBW can be improved through a trade-off design. The characteristics of resonance frequency, output power, and FBW of pMUT with different proof mass are analyzed with a piezoelectric layer of 1 μm and a structural layer of 5 μm. In this work, the far-field sound pressure is 240.5 Pa/V in water, 49.5 Pa/V higher than the traditional pMUT, benefiting from the piston diaphragm movement. Furthermore, a 23% −6 dB FBW in water is demonstrated by theoretical analysis and parameter optimization. This work provides constructive advice for pMUT for better performance of transmission and resolution.

INDEX TERMS Piezoelectric micromachined ultrasonic transducer (pMUT), piston mode, mass loading effect, frequency adjustment, fractional bandwidth

I. INTRODUCTION

Nowadays, ultrasound technology has been widely utilized in various fields, including medical imaging [1], non-destructive testing [2], and range-finding [3]. In particular, a piezoelectric micromachined ultrasonic transducer (pMUT) has attracted great attention due to its smaller size, lower cost and compatibility with complementary metal oxide semiconductor (CMOS) technology. More and more researchers have been devoted to improving its electromechanical coupling efficiency and transmission power. Akhbari *et al.* proposed a bending film manufacturing process to achieve high-sensitivity of 40 nm/V at the center of the diaphragm [4]. Rozen *et al.* reported a new method of concentric ventilation ring to redirect the sound pressure from the rear side to the front side [5], which achieved a 4.5 dB increase in SPL for a design with a 400 μm radius venting ring.

The enhancement of transmitting power and receiving sensitivity is always desirable. Traditional pMUT has a Gaussian-like mode shape which greatly limits the transmission capacity. Only the peak of the diaphragm reaches the maximum displacement in Gaussian-like mode shape. An effective way of increasing the radiation power is to enable a piston-like diaphragm movement. Specifically, the vibrating diaphragm becomes from curved one to a flat one so that more acoustic medium can be promoted, increasing the transmitting sensitivity. Wang *et al.* presented a pMUT with piston-like motion by etching holes to improve transmitting sensitivity up to 73 nm/V at 2.31 MHz [6]. Chen *et al.* demonstrated a new pMUT with V-shaped springs to localize the residual stress, resulting in a flat vibrating membrane [7]. Guedes *et al.* designed flexural suspended pMUT, showing a piston-like mode shape to improve output sound pressure [8]. However, the released holes on the active vibrating membrane will affect the reliability of pMUT.

In the ultrasonic transducer field such as therapeutics [9], spatial image resolution can be improved by simply transmitting and receiving shorter signals [10], [11], which proposes pMUT has a broadband characteristic. Recently,

many efforts have been made to improve the wide-band characteristics of pMUTs. Hajati *et al.* designed a pMUT array with different cavities radius to obtain a 55% FBW [12]. Wang *et al.* presented a mode-merging pMUT with a rectangular membrane to get a 95% FBW in water [17].

This paper proposes two new piston-like pMUTs by introducing a proof mass under the structure layer via simulations using COMSOL Multiphysics [13], and a standard finite element method (FEM) simulator is used for ultrasound propagation. Simulations performed using the FEM effectively analyze of problems that are difficult to solve using the wave equation. The structure of proof mass changes the mass and stiffness of the diaphragm. The resonance frequency can be adjusted by changing the size of the proof mass, which improves the design and application flexibility. A large ratio of third-order resonance frequency to first-order resonance frequency can be obtained by an additional proof mass under the circular diaphragm, which can realize low-frequency and high-frequency operation methods. A small ratio can be obtained by ring-proof mass which can realize a broad frequency band. The membrane remains flat during vibration by introducing a proof mass, resulting in a higher transmission sensitivity. The far-field pressure of 240.5 Pa/V is achieved for pMUT with larger h_2. Through a trade-off design, a -6 dB FBW as high as 23% is demonstrated.

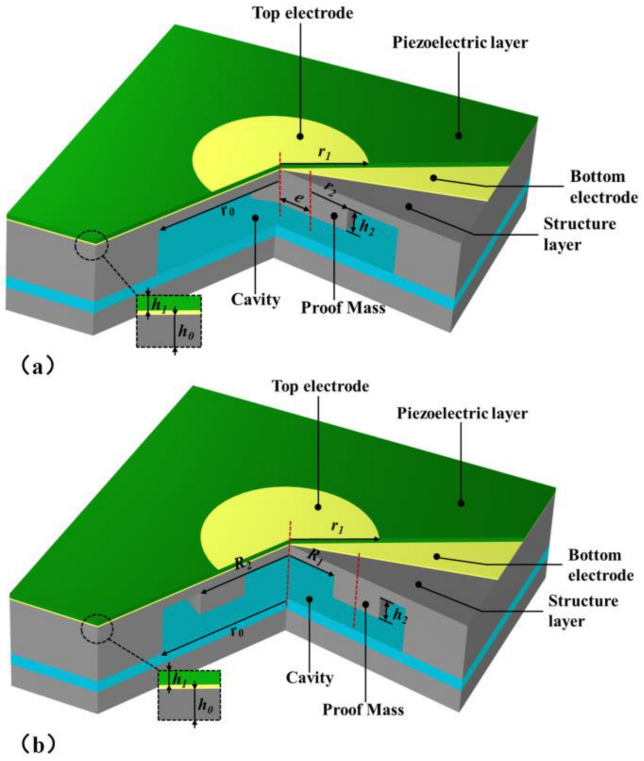

FIGURE 1. Design of two types piston-like pMUT 3-D schematics of (a) central cylindrical type piston-like pMUT and (b) ring cylindrical type piston-like pMUT.

II. CONCEPT AND DESIGN

A. STRUCTURE DESIGNING

The structure of the proposed pMUT is illustrated in Fig. 1 (a–b). It consists of a traditional circular diaphragm and proof mass under the structural layer. This work has two forms of proof mass: central cylindrical proof mass in Fig. 1(a) and ring cylindrical proof mass in Fig. 1(b). The circular diaphragm is designed with a silicon (Si) substrate and a thin Aluminium Nitride (AlN) film sandwiched by two electrodes (Mo). The proof mass is made of Si. The circular-shaped top electrode covers the piezoelectric layer with coverage of 65% used in traditional pMUT. This design ensures the maximum transmitting efficiency for pMUT [14]. As for piston-like pMUT, different electrode coverage for different strain profile is tightly coupled to the piezoelectric elecromechanical coupling efficiency, which is analyzed in the following sections. Considering the influence of frequency, sensitivity and half wavelength on the performance of the device and subsequent applications, the AlN layer (h_1) and Si layer (h_0) thickness are set as 1 μm and 5 μm, respectively. An ideal piston membrane movement can be obtained by adjusting the size of the proof mass. The piston vibration mode can push more acoustic medium to produce ultrasonic wave than traditional Gaussian-like mode shapes when the voltage is applied to the electrodes.

In this section, a simplified lumped model is established with mass, spring and damper. In Section III, IV, and V, a systematic simulation is carried out to verify the theoretical model. Table 1 and Table 2 summarize the structure and materials parameters for the piston-like pMUT investigated in this work.

TABLE 1. Summary of the structure parameters of the analyzed pMUT.

Symbol	Value	Unit	Description
r_0	200	μm	Cavity radius
r_1	$0.65*r_0$	μm	Top electrode radius
r_2	/	μm	Center-proof mass radius
R_1	/	μm	Ring-proof mass inner radius
R_2	/	μm	Ring-proof mass outer radius
h_0	5	μm	Structure layer thickness
h_1	1	μm	Piezoelectric layer thickness
h_2	/	μm	Proof mass thickness
e	0	μm	Proof mass eccentricity

All symbols are illustrated in Fig. 1.

TABLE 2. Summary of the material properties.

Symbol	Value	Unit	Description
Y_1	*170*	*GPa*	Young's modulus of Si
Y_2	*340*	*GPa*	Young's modulus of AlN
v_1	*0.28*	/	Poisson's ratio of Si
v_2	*0.3*	/	Poisson's ratio of AlN
ρ_1	*2329*	kg/m^3	Density of Si
ρ_2	*3300*	kg/m^3	Density of AlN
d_{31}	*2.2*	*pm/V*	Piezoelectric coefficient of AlN

A fabrication process of piston-mode pMUT is designed, as shown in Fig. 2: (a) Cavity radius of capping wafer is fabricated according to the designed pMUT geometry; (b) The

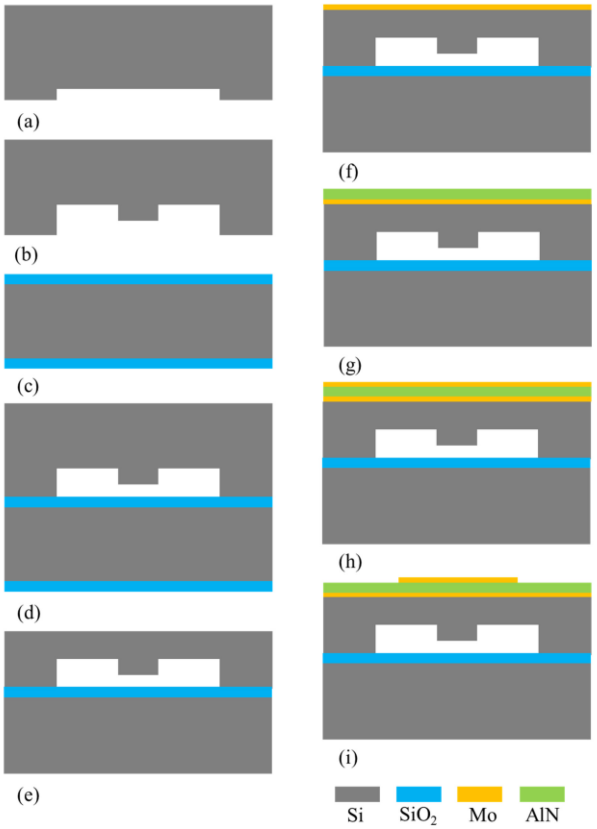

FIGURE 2. Fabrication process of piston-mode pMUT.

shape of the proof mass is etched in the middle of the circular diaphragm, the etch depth is controlled by etch time; (c) Handle wafer is thermally oxidized; (d) After cavity fabrication and buried oxide formation, capping wafer is bonded to handle wafer with direct bonding at $1x10^{-3}$ mbar, which is kept as a constant pressure in all the trials. The bonding is preceded by a standard cleaning procedure of two wafers; (e) Subsequently, the bonded wafer is annealed at 1100 °C for 2 h in a diffusion furnace after which the top wafer is thinned down by grinding and the Chemical and Mechanical Polishing (CMP). The grinding is conducted on wafer back grinder using diamond cup coarse and fine wheels. The polishing is carried out with a commercial CMP tool using standard polishing pads and slurries for silicon. A double side mask aligner is used for the transfer of backside alignment marks; (f)-(h) Mo electrodes (100nm-thick) and piezoelectric AlN layer (1μm-thick) are deposited on the structure layer (5μm-thick); (i) Mo top electrode (100nm-thick) patterning with photoresist (PR).

Only a lithograph process in step (a) is added to the fabrication process of piston-mode pMUT compared with the traditional pMUT fabrication process. This piston-like pMUT has advantages compared to traditional pMUT due to the design flexibility of proof mass. The shape, thickness, eccentricity and radius of the proof mass can be adjusted independently.

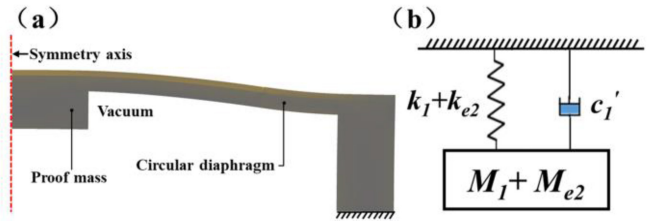

FIGURE 3. Working mechanism of the piston-like pMUT. (a) Cross-section schematic of the piston-like pMUT cell. (b) Simplified two degrees of freedom lumped model.

B. LUMPED MODEL FOR PISTON-LIKE pMUT CELL

A lumped element model can be taken to analyze the vibration behavior of the piston-like pMUT cell due to the dimension of the pMUT is small than that of the acoustic wavelength. The cross-section schematic of the piston-like pMUT is shown in Fig. 3(a), and the two degrees of freedom model is established as shown in Fig. 3(b) [15]. The piezoelectric effect of AlN diaphragm sandwiched between the top and bottom electrodes produces the in-plane transverse stress. Then a flexural moment is generated to deflect the diaphragm.

The cavity between the diaphragm and substrate is assumed to be a vacuum. M_1 and k_1 in Fig. 3(b) represent the lumped mass and spring of the circular diaphragm without proof mass, respectively. M_{e2} and k_{e2} are equivalent mass and spring introduced by the additional proof mass to the circular diaphragm. c_1' is equivalent material damping coefficient. The mass and stiffness of the circular diaphragm can be adjusted by the addition of proof mass, which changes the resonance frequency of the piston-like pMUT. The resonance frequency can be obtained by the simplified two degrees of freedom lumped model as:

$$f_p = \frac{1}{2\pi}\sqrt{\frac{k_1 + k_{e2}}{M_1 + M_{e2}}}. \tag{1}$$

C. VIBRATION MODE OF THE PISTON-LIKE pMUT

A central proof mass making of Si is added to a circular diaphragm, changing the geometry of the membrane in the vertical direction to obtain an ideal piston membrane movement without significantly increasing the complexity of the manufacturing process or reducing device yield. As the increase in proof mass dominates the mass and stiffening of the membrane, the central region of the diaphragm is subject to slight deflection and remains flat.

Most noticeably, compared with traditional pMUT, the piston-like pMUT has greater design flexibility. The structural parameters of proof mass can be designed independently for diaphragm thickness and radius. The elastic coefficient and diaphragm mass can be decoupled from each other. As for traditional pMUT, only the center of the circular diaphragm can achieve maximum displacement due to the Gaussian-like vibration mode. Benefited from an additional proof mass whether center-proof mass or ring-proof

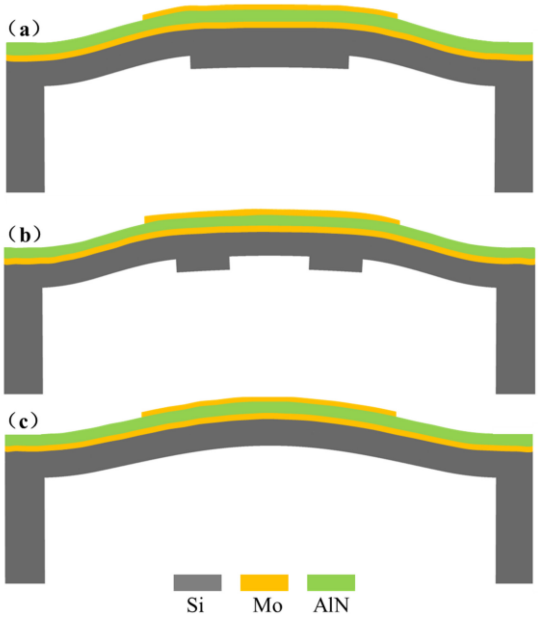

FIGURE 4. Mode shape diagram obtained by finite element simulation: (a) Center-proof mass piston-like pMUT mode shape; (b) Ring-proof mass piston-like pMUT mode shape; (c) Traditional pMUT mode shape.

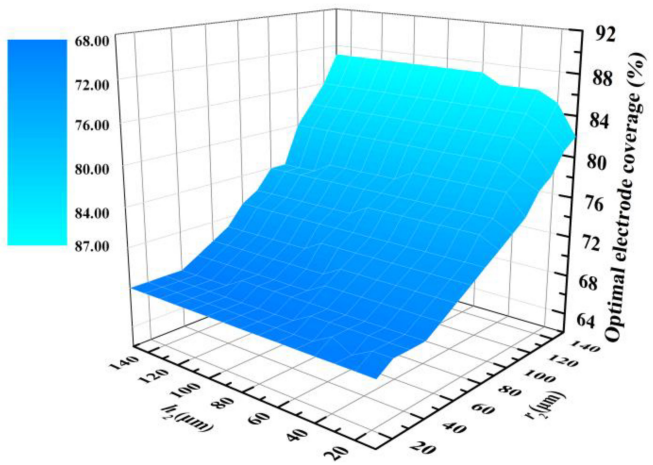

FIGURE 5. The relationship between optimal electrode coverage of the piston-like pMUTs with center-proof mass.

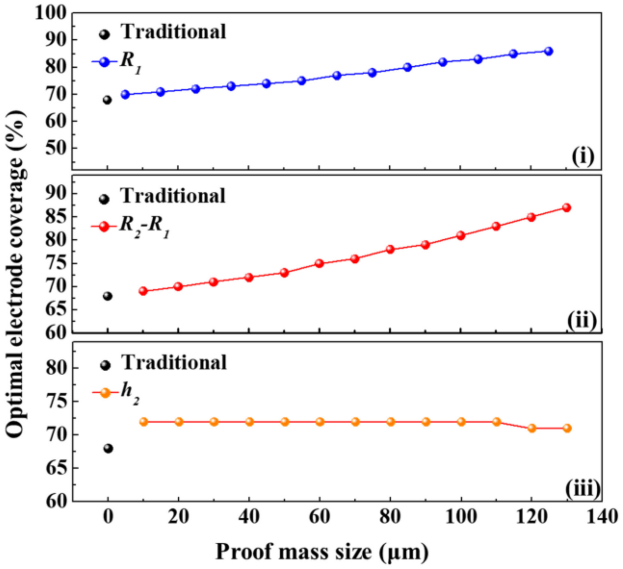

FIGURE 6. The relationship between optimal electrode coverage of the piston-like pMUTs with ring-proof mass. (i) The relationship between optimal electrode coverage with different R_1 when R_2-R_1 and h_2 is fixed as 40μm and 20μm, respectively; (ii) The relationship between optimal electrode coverage with different R_2-R_1 when R_1 and h_2 is fixed as 30μm and 20μm, respectively; (iii) The relationship between optimal electrode coverage with different h_2 when R_1 and R_2-R_1 is fixed as 30μm and 40μm, respectively.

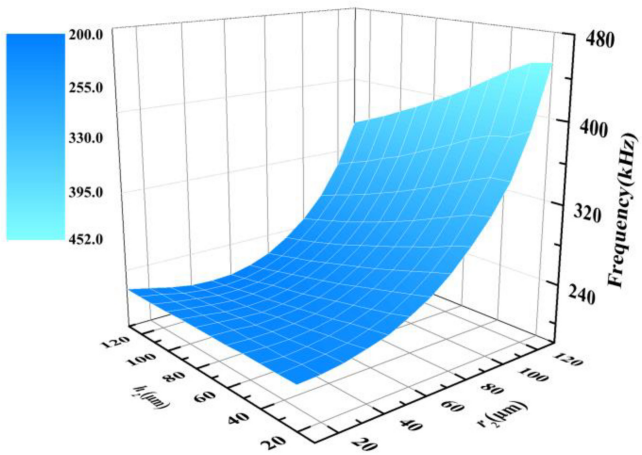

FIGURE 7. The relationship between resonance frequency of piston-like pMUT with the size of center-proof mass.

mass, the mode shape of piston-like pMUT has more uniform diaphragm displacement than the traditional one as shown in Fig. 4(a) and (b), showing a larger effective area. The central region moves up and down like a piston.

As shown in Fig. 5, the optimal electrode coverage under the different size of the proof mass is demonstrated. The optimal electrode coverage increases with an increase of r_2 when h_2 is fixed, and a larger effective area is achieved. On the contrary, the optimal electrode coverage does not fluctuate with different h_2 when r_2 is fixed, and it can be regarded as a constant. As for ring-proof mass, the optimal electrode coverage increases with R_1 and R_2-R_1 increasing when h_2 is fixed as 20μm as shown in Fig. 6. The variation trend of the optimal electrode coverage with the thickness of the ring-proof mass is consistent with the trend of the center-proof mass, showing a fixed effective transmission area.

III. DISCUSSION OF FREQUENCY CHARACTERISTICS

A. DISCUSSION OF CENTER-PROOF MASS PISTON-LIKE pMUT

The variation resonance frequency can be seen in Fig. 7 obtained by changing the radius and thickness of the center-proof mass. Resonance frequency goes down with the increase of h_2 since the ruling effect is diaphragm mass. The resonance frequency increases as the stiffness of the diaphragm dominates.

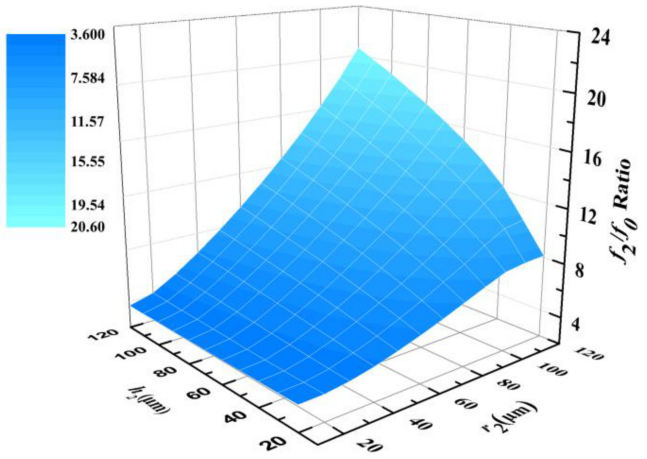

FIGURE 8. The relationship between ratio of (0, 0) and (2, 0) resonance frequency of piston-like pMUT with the size of center-proof mass.

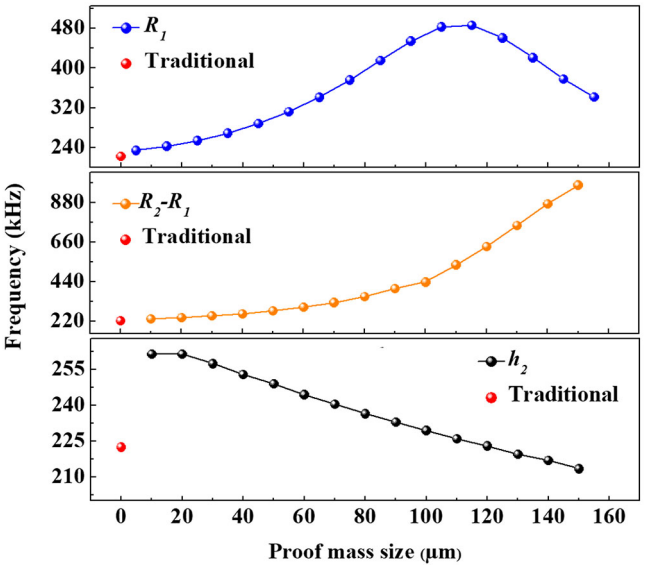

FIGURE 9. The relationship between resonance frequency of piston-like pMUT with the size of ring-proof mass when R_1, R_2-R_1, and h_2 are fixed as 30 μm, 40 μm, and 20μm, respectively.

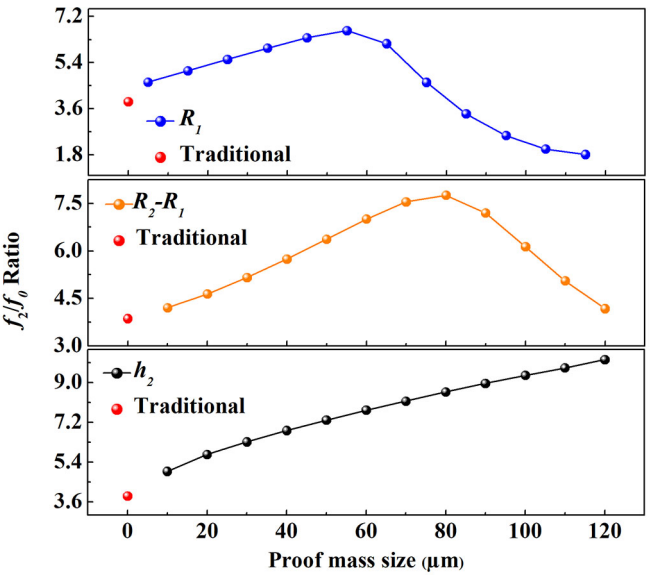

FIGURE 10. The relationship between ratio of (0, 0) and (2, 0) resonance frequency of piston-like pMUT with the size of ring-proof mass when R_1, R_2-R_1, and h_2 are fixed as 30 μm, 40 μm, and 20μm, respectively.

For rectangular-shaped pMUT used in a dual-frequency application, both (0, 0) and (2, 0) vibration modes of the rectangular membrane can be used efficiently if electrode shapes are properly designed [16]. The (0, 0) and (2, 0) resonance frequency ratio need to be adjusted within a wide range. The ratio of (0, 0) and (2, 0) resonance frequency of piston-like pMUT can be adjusted by the size of center-proof mass compared with traditional pMUT, as shown in Fig. 8. The frequency ratio is proportional to the size of the center-proof mass, including the radius and thickness of the center-proof mass.

B. DISCUSSION OF RING-PROOF MASS PISTON-LIKE pMUT

As for ring-shaped proof mass piston-like pMUT, there are three important parameters to adjust the frequency of the pMUT, including the ring-proof mass inner radius (R_1), the difference between the ring-proof mass outer radius and the ring-proof mass inner radius (R_2-R_1), and ring-proof mass thickness (h_2). Through the trade-off design of diaphragm stiffness and mass, the resonance frequency of piston-like pMUT increases first and then decreases by changing the R_1 when the (R_2-R_1) and h_2 are fixed as 40 μm and 20 μm as shown in Fig. 9. What's more, the resonance frequency of the piston-like pMUT presents a trend that is proportional to (R_2-R_1) when R_1 and h_2 are fixed as 30 μm and 20μm respectively, and inversely proportional to h_2 when (R_2-R_1) and R_1 are fixed as 40 μm and 30 μm respectively.

The ratio of (0, 0) and (2, 0) resonance frequency of ring-proof mass piston-like pMUT has a smaller adjustment range than that of center-proof mass piston-like pMUT. The smallest frequency ratio shown in Fig. 10 is 1.816 with a circular diaphragm in this work when R_1 equals 115 μm. The first a few resonance frequencies are closer to each other with an additional ring-proof mass of the rectangular plate. Therefore, a broad frequency band can be formed when the resonant peaks of different vibration modes are merged together in liquid-coupled operation including water and FC-84, etc. [17].

In summary, the resonance frequency of the transducer can be adjusted by proof mass, which increases the flexibility of design. Furthermore, the largest ratio of (0, 0) and (2, 0) resonance frequency can be obtained by center-proof mass piston-like pMUT, while the smallest one can be obtained by piston-like pMUT with ring-proof mass. Therefore, the dual-frequency and broadband operation methods can be achieved by piston-like pMUT.

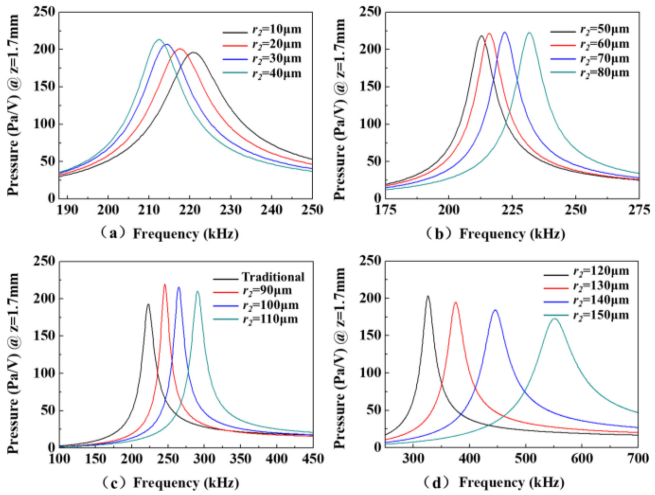

FIGURE 11. The relationship between far-field pressure response (z = 1.7mm) with different center-proof mass radius when h_2 is fixed as 100 μm. (a) Pressure curves with r_2 = 10 – 40 μm. (b) Pressure curves with r_2 = 50 – 80 μm. (c) Pressure curves with r_2 = 90 – 110 μm and traditional pMUT. (d) Pressure curves with r_2 = 120 – 150 μm.

IV. DISCUSSION OF TRANSMITTING SENSITIVITY

In order to further explore the impact of proof mass size on the transmitting sensitivity of piston-like pMUT, a systematic simulation has been made to optimize the size of the proof mass. The acoustic-piezoelectric interaction, frequency domain package in COMSOL software is used in FEM model. The quadrilateral mesh elements are drawn over the x-y plane and swept along the z-direction. The mesh elements in each domain are determined with the resonant frequency and material properties. As a result, the number of degrees of freedom is about 0.25 million in the electromechanical-acoustic analysis. For an accurate evaluation of the output pressure, the proposed pMUT is immersed in water. An acoustic domain and an acoustic PML (Perfect Matching Layer) are used to simulate the electric impedance and acoustic field under water. In order to make the figures clearer, no more than five curves are placed in one figure.

A. DISCUSSION OF CENTER-PROOF MASS PISTON-LIKE pMUT

Firstly, r_2 and h_2 are varied to establish the relationship between the proof mass dimension and the piston-like pMUT transmitting sensitivity. In this case, the thickness of the center-proof mass is determined as 100 μm. As shown in Fig. 11, the 1st resonance frequency of the circular diaphragm is analyzed with the variation of different r_2.

To further explore the impact of proof mass size on the transmitting sensitivity of transducer, the surface pressure of a pMUT is given by [18]:

$$P = VZ\sqrt{n} \tag{2}$$

where V is the volume velocity of the circular diaphragm, Z is the acoustic impedance of acoustic medium, and n is the array fill-factors of the pMUT array. The volume velocity is related to the diaphragm displacement and the effective area of the diaphragm. As for a single pMUT, higher diaphragm displacement and larger effective area can produce higher volume velocity and higher sound pressure output. For a traditional clamped pMUT, the effective diaphragm area presents the one-third value of the circular diaphragm area due to the Gaussian-like mode shape. As for piston-like pMUT with center-proof mass, the effective diaphragm area increases with increasing r_2. However, the diaphragm displacement amplitude decreases sharply with larger r_2. So, the far-field pressure of piston-like pMUT goes up initially and then it begins to decreases as shown in Fig. 11.

The maximum displacement increases with the center-proof thickness increasing under the same driven voltage compared with the traditional pMUT. As for a circular clamped membrane with radius r_0, the static deflection $d(x)$ under the driven voltage can be expressed as [19]:

$$d(x) = d_0 w(x) \tag{3}$$

where $x = r/r_0$ is the normalized radial coordinate, d_0 is the peak deflection, and $w(x)$ is the normalized mode-shape. The traditional pMUT has a Gaussian-like vibration mode shape, and the pMUT proposed in this paper has a piston vibration mode shape.

The stiffness of the pMUT membrane, k can be obtained as:

$$k = 18\pi D I_e / a^2 \tag{4}$$

where I_e is an integral related to the elastic strain for mode shape and D is flexural rigidity of the plate obtained from:

$$D = \int \frac{E(z)z^2}{1 - v(z)^2} dz \tag{5}$$

where $E(z)$ is Young's Modules and $v(z)$ is Poisson's ratio of the material at a distance z form the neutral axis, which is the point where the sum of stresses is equal to zero. The integration is conducted for z varying form the bottom to the top of the plate.

A pMUT can be modeled using an equivalent circuit model with two transformers [20]: electromechanical and mechanical-acoustic coupling transformers. The former transformer can be expressed:

$$F_{in} = \eta V_{in} \tag{6}$$

where V_{in} is the input voltage, F_{in} is the effective piezoelectric force and η is the transformer ratio:

$$\eta = \frac{1}{2} e_{31,f} z_p I_{piezo} \tag{7}$$

where $e_{31,f}$ is the effective thin-film piezoelectric coefficient, z_p is the distance from the center of the piezoelectric layer to the neutral axis of the membrane, and I_{piezo} is an integral that captures the effect of the electrode layout and particular mode-shape. I_{piezo} goes up initially and approximates a constant with larger h_2 when r_2 is fixed. Moreover, the effective thin-film piezoelectric coefficient is stable when the

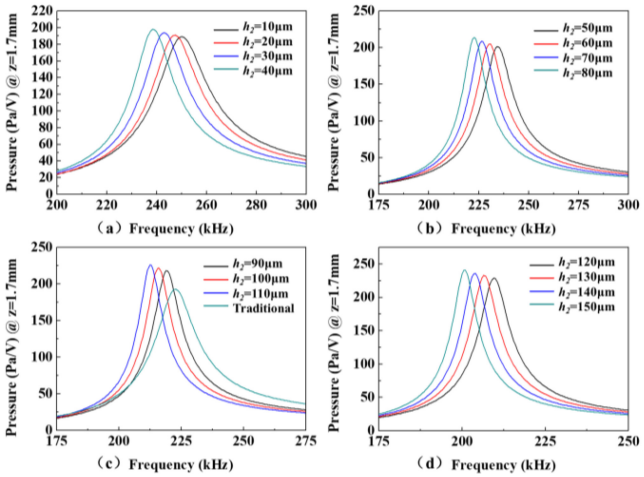

FIGURE 12. The relationship between far-field pressure response (z = 1.7mm) with different center-proof mass thickness when r_2 is fixed as 60 μm. (a) Pressure curves with $h_2 = 10 - 40$ μm. (b) Pressure curves with $h_2 = 50 - 80$ μm. (c) Pressure curves with $h_2 = 90 - 110$ μm and traditional pMUT. (d) Pressure curves with $h_2 = 120 - 150$ μm.

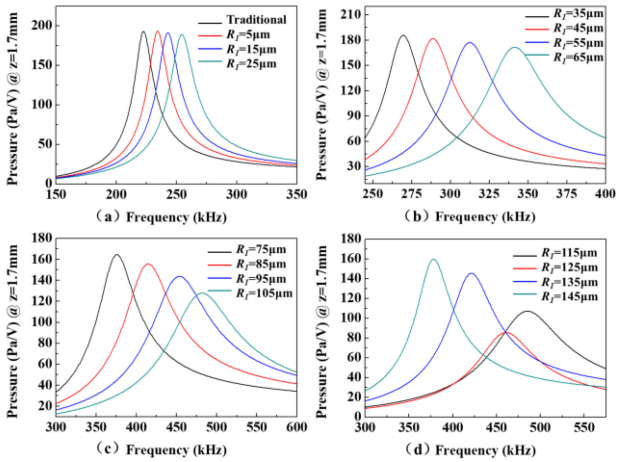

FIGURE 13. The relationship between far-field pressure response (z = 1.7mm) with different ring-proof mass when R_2-R_1 and h_2 are fixed as 40 μm and 20 μm, respectively. (a) Pressure curve with $R_1 = 5 - 25$ μm and traditional pMUT. (b) Pressure curve with $R_1 = 35 - 65$ μm. (c) Pressure curve with R_1=75-105 μm. (d) Pressure curve with $R_1 = 115 - 145$ μm.

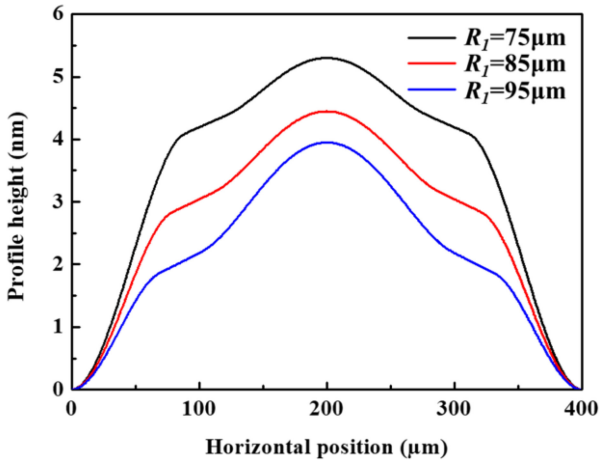

FIGURE 14. The relationship between surface profiles of the piston-like pMUTs with $R_1 = 75 - 95$ μm when R_2-R_1 and h_2 are fixed as 40μm and 20μm.

piezoelectric material is selected. So, the transformer ratio is determined by the I_{piezo} and z_p. The distance from piezoelectric layer to the neutral axis of the membrane increases with the center-proof and ring-proof mass thickness increasing. Therefore, the maximum displacement increases although the stiffness of the pMUT slightly increases. Therefore, the maximum displacement of the circular diaphragm of the piston-like pMUT increases firstly with the increase of z_p and I_{piezo}, and then decreases due to the larger stiffness and invariant I_{piezo} when r_2 is fixed.

Due to the diaphragm displacement amplitude increases with effective diaphragm area changing slightly, the far-field pressure increases as the thickness of proof mass increases in a specific range when r_2 is fixed as 60 μm, as shown in Fig. 12. Moreover, on the basis that current MEMS technology can get a deep cavity of cavity-SOI (CSOI) wafer or SOI wafer within a specific range, the larger the thickness of proof mass, the better. As expected, the piston-like pMUT exhibits higher transmitting sensitivity by optimizing r_2 and h_2 of center-proof mass. In contrast, far-field pressure reaches as high as 240.5 Pa/V in water which is 49.5 Pa/V higher than traditional pMUT.

B. DISCUSSION OF RING-PROOF MASS PISTON-LIKE pMUT

As for ring-proof mass piston-like pMUT, an important parameter of the ring-proof mass inner radius is different from center-proof mass piston-like pMUT as shown in Fig. 13. The diaphragm displacement amplitude and effective diaphragm area decrease with larger R_1, as shown in Fig. 14. The inner region of the ring-proof mass is close to Gaussian-like mode shape with larger R_1 which limits the transmitting sensitivity. Nevertheless, the transmitting sensitivity increases with increasing displacement for a larger inner radius of ring-proof mass, as shown in Fig. 13(d).

Therefore, increasing the thickness of the ring or the center-proof mass is an effective method to improve the transmitting sensitivity of the piston-like pMUT. For increasing the width of the proof mass, the transmitting sensitivity decreases as the displacement decreases, although the effective area increases. Furthermore, piston-like vibration mode changes into Gaussian-like vibration mode with a larger inner radius of ring-proof mass, limiting the transmitting sensitivity.

V. DISCUSSION OF BROADBAND OPTIMIZATION

This section discusses the broadband characteristics of piston-like pMUT with center and ring-proof mass and traditional pMUT in liquid-coupled operation. The key to

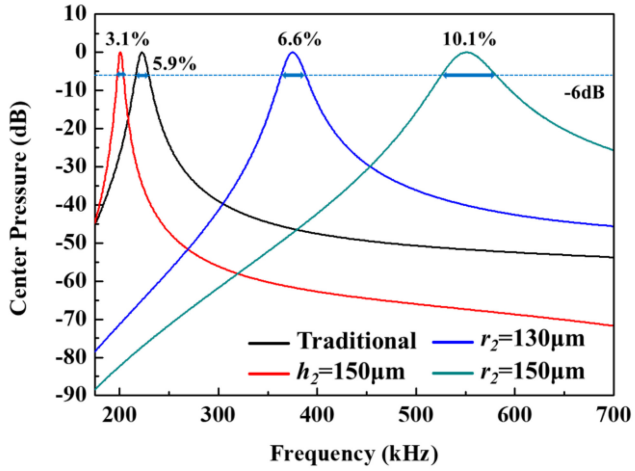

FIGURE 15. The relationship between pressure-frequency response of traditional pMUT and piston-like pMUT with center-proof mass in water and −6 dB bandwidth with different center-proof mass size when h_2 and r_2 are fixed as 100 μm and 60 μm, respectively.

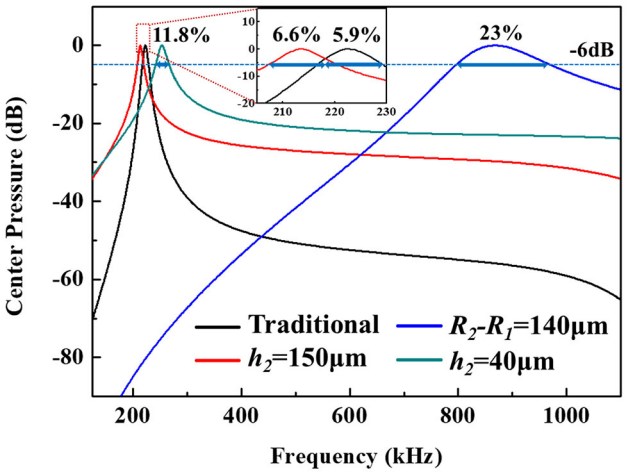

FIGURE 16. The relationship between pressure-frequency response of traditional pMUT and piston-like pMUT with ring-proof mass in water and −6 dB bandwidth with different ring-proof mass size when R_1, R_2-R_1, and h_2 are fixed as 30 μm, 40 μm, and 20 μm, respectively.

adjusting the bandwidth of piston-like pMUT in this paper is to control the size of the proof mass. As shown in Fig. 15, the FBW, defines as the −6 dB frequency range divided by the resonance frequency ($BW_f = \Delta f/f_0$), which varies significantly based on the acoustic medium and proof mass size. When an acoustic medium is water, the FBW of center-proof mass pMUT can change from 3.1% to 10.1% with h_2 and r_2 equaling 150 μm respectively while the FBW of traditional pMUT is 5.9%. While high sensitivity can be achieved by thickening center-proof mass, the FBW obtained as a result is narrow. The narrow band and high sensitivity characteristics of piston-like pMUT are suitable for sensing applications when using continuous waves but are not suitable for imaging using pulse echoes. When r_2 exceeds 100 μm, the sensitivity of the transducer is larger than traditional pMUT. A piston-like pMUT with a wider proof mass can receive shorter pulses than the traditional pMUT.

Bandwidth characteristic is demonstrated in piston-like pMUT with ring-proof mass as shown in Fig. 16. When the inner radius of ring-proof mass exceeds 100 μm, the transmitting sensitivity decreases sharply. Moreover, the transmitting sensitivity minimized when (R_2-R_1) is 140 μm. In the vicinity of this inner and outer radius, the bandwidth of the device expands rapidly which the largest one is 23%.

As analyzed above, piston-like pMUT can reach a narrow frequency band with center-proof mass and a broad frequency band with ring-proof mass. In general, there is a trade-off relationship between the sensitivity and the device bandwidth. However, in this device, no significant reduction in the bandwidth is observed. Moreover, in ultrasonic imaging, as the signal then becomes shorter in terms of time with broader bandwidth becoming, and, as a result, high-resolution images can be acquired. Therefore, the pMUT with center-proof mass and ring-proof mass can be applied to high sensitivity and high-resolution applications, respectively. Compared with traditional pMUT, a larger bandwidth can be obtained in pMUT with proof mass when the transmission sensitivity is close, as shown in Table 3.

VI. DISCUSSION OF TWO STRUCTURES

In this paper, two structures of piston-like pMUTs are designed with center-proof mass and ring-proof mass. Benefited from piston-like vibration mode, the proposed pMUTs have more uniform diaphragm displacement than the traditional one and show larger effective area. In order to realize the use of ultrasonic in long-distance underwater imaging, the effects of proof mass on the frequency characteristics and optimal electrode coverage of the proposed pMUTs have been studied. The configurations of two different structures will be flexibly applied in complex scenarios.

Compared with traditional pMUT, the piston-like pMUT has greater design flexibility. The structure parameters of proof mass can be designed independently for diaphragm thickness and radius. The elastic coefficient and diaphragm mass can be decoupled from each other. Therefore, the resonance frequency of the proposed pMUT can be adjusted by proof mass, which increases the design flexibility.

The largest ratio of third-order to first-order resonance frequency can be obtained with center-proof mass. Therefore, both (0, 0) and (2, 0) vibration modes can be efficiently used with well-designed electrode shapes. The smallest frequency ratio (1.8) can be obtained with ring-proof mass. So, the first a few resonance frequencies are closer to each other, especially with the rectangular plate. A broad frequency band can be formed when the resonant peaks of different vibration modes are merged in liquid-coupled operation.

By theoretically analyzing and optimizing parameters, the largest far-field sound pressure of 240.5 Pa can be obtained with larger thickness of proof mass. The largest FBW of 23% can be obtained with ring-proof mass. Therefore, the

TABLE 3. The results of the traditional pMUT and proposed pMUT.

r_2 (μm)	R_1 (μm)	R_2-R_1 (μm)	h_2 (μm)	*Pressure* (Pa/V)	*FBW*
/	/	/	/	192.8	5.9%
60	/	/	150	240.5	3.1%
/	30	140	20	120.2	23%
130	/	/	100	194.6	6.6%
/	30	40	150	231.7	6.6%
/	30	40	40	193.2	11.8%
/	30	40	170	240	6%
120	/	/	100	203	5.6%

pMUT with larger thickness of proof mass has larger detection range and higher transmission sensitivity. The pMUT with ring-proof mass has a smaller detection blind area, higher resolution and larger bandwidth. The proposed pMUT with larger thickness of proof mass for long-distance detection application has a great advantage of higher transmission sound pressure. The proposed pMUT with ring-proof mass has greater application potential for short-range imaging application due to the broad frequency band and smaller detection blind area. Furthermore, more data show a larger bandwidth can be obtained in the pMUT with ring-proof mass when the transmission sensitivity is close compared with traditional pMUT, as shown in Table 3. Meanwhile, higher far-field sound pressure is presented in the proposed pMUT with ring-proof mass under the similar FBW of traditional pMUT.

The proposed method has guiding significance for pMUT design. First of all, the resonant frequency can be adjusted by proof mass. The thickness of the diaphragm and the diameter of the cavity are decoupled. Specific thickness can be used to meet the requirements of the manufacturing process. A suitable diameter can be chosen to meet the half-wavelength limitation of the pMUT array. The proof mass can be used to compensate for the frequency difference with the target frequency. Then, the theoretical mechanism and regulation law of proof mass improving transmission performance have been studied and summarized. The optimal electrode coverage increases with increase of the radius of proof mass. On the contrary, the optimal electrode coverage does not fluctuate with the thickness of the proof mass. During the design of piston-like pMUT by the proposed method, the optimal electrode coverage needs to be specially selected to achieve maximum transmission efficiency. According to the law summarized in this paper, the size and shape of proof mass can be flexibly selected. Therefore, the pMUT with better performance can meet the target by adding a proof mass.

VII. CONCLUSION

A novel pMUT with proof mass is proposed in this paper. The finite element simulation results show that the proposed piston-like pMUT can adjust the resonance frequency and increase design flexibility compared with traditional pMUT. Meanwhile, A large ratio of third-order resonance frequency to first-order resonance frequency can be obtained to realize low-frequency and high-frequency operation methods. In addition, the piston-like pMUT has a flat surface during vibration due to the proof mass, which increases effective area and improves transmitting performance. The far-field pressure is 49.5 Pa/V higher than a traditional pMUT, and a 23% −6 dB FBW is demonstrated based on the theoretical analysis and parameter optimization. Moreover, using wafer bonding technology to produce proof mass does not increase the process complexity sharply in CSOI wafer manufacturing technology. This piston-like pMUT with proof mass may become an alternative to the next-generation ultrasonic transducer.

REFERENCES

[1] Y. Yang *et al.*, "An ultra-high element density pMUT array with low crosstalk for 3-D medical imaging," *Sensors*, vol. 13, no. 8, pp. 9624–9634, 2013.

[2] P. Muralt and J. Baborowski, "Micromachined ultrasonic transducers and acoustic sensors based on piezoelectric thin films," *J. Electroceram.*, vol. 12, no. 1, pp. 101–108, 2004.

[3] R. J. Przybyla *et al.*, "In-air rangefinding with an ALN piezoelectric micromachined ultrasound transducer," *IEEE Sensors J.*, vol. 11, no. 11, pp. 2690–2697, Nov. 2011.

[4] S. Akhbari, F. Sammoura, C. Yang, A. Heidari, D. Horsley, and L. Lin, "Self-curved diaphragms by stress engineering for highly responsive pMUT," in *Proc. MEMS*, 2015, pp. 837–840.

[5] O. Rozen, S. T. Block, S. E. Shelton, and D. A. Horsley, "Piezoelectric micromachined ultrasonic transducer with increased output pressure via concentric venting rings," in *Proc. TRANSDUCERS*, 2015, pp. 670–673.

[6] T. Wang, R. Sawada, and C. Lee, "A piezoelectric micromachined ultrasonic transducer using piston-like membrane motion," *IEEE Electron Device Lett.*, vol. 36, no. 9, pp. 957–959, Sep. 2015.

[7] X. Chen, D. Chen, X. Liu, D. Yang, J. Pang, and J. Xie, "Transmitting sensitivity enhancement of piezoelectric micromachined ultrasonic transducers via residual stress localization by stiffness modification," *IEEE Electron Device Lett.*, vol. 40, no. 5, pp. 796–799, May 2019.

[8] A. Guedes, S. Shelton, R. Przybyla, I. Izyumin, B. Boser, and D. A. Horsley, "Aluminum nitride pMUT based on a flexurally-suspended membrane," in *Proc. 16th Int. Solid-State Sens. Actuat. Microsyst. Conf.*, 2011, pp. 2062–2065.

[9] H.-Y. Tang, Y. Lu, S. Fung, D. A. Horsley, and B. E. Boser, "11.8 Integrated ultrasonic system for measuring body-fat composition," in *IEEE Int. Solid-State Circuits Conf. (ISSCC) Dig. Tech. Papers*, 2015, pp. 1–3.

[10] H. Taki, K. Taki, M. Yamakawa, T. Shiina, M. Kudo, and T. Sato, "High-range-resolution imaging using frequency domain interferometry with stabilization techniques for real-time vascular ultrasound," *Jpn. J. Appl. Phys.*, vol. 54, no. 7S1, 2015, Art. no. 07HF05.

[11] R. Lerch, and W. Friedrich, "Ultrasound fields in attenuating media," *J. Acoust. Soc. America*, vol. 80, no. 4, pp. 1140–1147, 1986.

[12] A. Hajati *et al.*, "Three-dimensional micro electromechanical system piezoelectric ultrasound transducer," *Appl. Phys. Lett.*, vol. 101, no. 25, 2012, Art. no. 253101.

[13] L. Wang, J. Zhou, W. Zhu, Z. Wu, W. Liu, and C. Sun, "A novel piston-like piezoelectric micromachined ultrasonic transducer based on mass loading effect," in *Proc. EDTM*, 2021, pp. 1–3.

[14] P. Muralt *et al.*, "Piezoelectric micromachined ultrasonic transducers based on PZT thin films," *IEEE Trans. Ultrason., Ferroelect., Freq. Control*, vol. 52, no. 12, pp. 2276–2288, Dec. 2005.

[15] S. Na, L. L. P. Wong, A. I. H. Chen, Z. Li, M. Macecek, and J. T. W. Yeow, "Lumped element modeling of air-coupled capacitive micromachined ultrasonic transducers with annular cell geometry," *Ultrasonics*, vol. 76, pp. 19–27, Apr. 2017.

[16] C. Chao, T.-Y. Lam, K.-W. Kwok, and H. Lai-Wa Chan, "Piezoelectric micromachined ultrasonic transducers with rectangular diaphragms for dual-frequency applications," in *Proc. Micro (MEMS) Nanotechnol. Defense Security*, 2007, Art. no. 65561J.

[17] T. Wang, T. Kobayashi, and C. Lee, "Micromachined piezoelectric ultrasonic transducer with ultra-wide frequency bandwidth," *Appl. Phys. Lett.*, vol. 106, no. 1, 2015, Art. no. 13501.

[18] G.-L. Luo and D. A. Horsley, "Piezoelectric micromachined ultrasonic transducers with corrugated diaphragms using surface micromachining," in *Proc. 20th Int. Conf. Solid-State Sens. Actuat. Microsyst. Eurosens. XXXIII*, 2019, pp. 841–844.
[19] Y. Lu, Q. Wang, and D. A. Horsley, "Piezoelectric micromachined ultrasonic transducers with increased coupling coefficient via series transduction," in *Proc. IEEE Int. Ultrasonics Symp.*, 2015, pp. 1–4.
[20] Y. Lu, A. Heidari, and D. A. Horsley, "A high fill-factor annular array of high frequency piezoelectric micromachined ultrasonic transducers," *J. Microelectromech. Syst.*, vol. 24, no. 4, pp. 904–913, 2014.

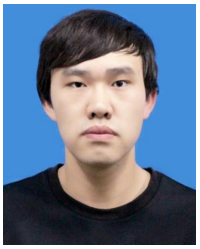

LEI WANG (Member, IEEE) received the B.E. degree in vehicle engineering from the Wuhan University of Technology, Wuhan, China, in 2019. He is currently pursuing the M.S. degree in mechatronic engineering with Wuhan University, Wuhan.

His current research interests include design and manufacture of pMUTs and lamb wave resonators.

JIE ZHOU (Member, IEEE) received the B.E. degree in mechanical engineering from Wuhan University, Wuhan, China, in 2018, where he is currently pursing the Ph.D. degree in mechanical and electronic engineering.

His major research direction is the design and manufacture of lamb wave resonators, sensors, and filters.

WEI ZHU (Member, IEEE) received the B.E. degree in mechanical engineering from Wuhan University, Wuhan, China, in 2019, where he is currently pursuing the M.S. degree in mechatronic engineering.

His current research interests include design and manufacture of piezoelectric micromachined ultrasonic transducers and acoustic wave-based sensors.

ZHIPENG WU received the B.E. degree in mechanical engineering from Wuhan University, Wuhan, China, in 2016, where he is currently pursing the Ph.D. degree in mechanical and electronic engineering. His research interests include of the thin film aluminum nitride-based piezoelectric micromachined ultrasonic transducers and their application.

WENJUAN LIU (Member, IEEE) received the B.E. and M.E. degrees from Tianjin University, Tianjin, China, in 2011 and 2014, respectively, and the Ph.D. degree in microelectronics from Fudan University, Shanghai, China, in 2020.

She is currently an Assistant Professor with The Institute of Technological Sciences, Wuhan University. Her research interests include modeling, design, and fabrication of AlN-based piezoelectric micromachined devices and systems for a range of industrial and medical applications.

CHENGLIANG SUN received the B.S. and Ph.D. degrees in physics from Wuhan University, Wuhan, China, in 1999 and 2006, respectively. From September 2004 to May 2011, he was a Research Associate with The Hong Kong Polytechnic University, a Postdoctoral Associate with the University of Pittsburgh, and a Fellow of the University of Wisconsin-Madison, WI, USA.

In May 2011, he joined the Institute of Microelectronics, A*STAR, and had been a Principle Investigator. In September 2017, he joined Wuhan University as a Professor and the Deputy Director of The Institute of Technological Sciences. His current research interests include the RF resonators and filters, SAW/BAW/MEMS sensors, and ultrasound transducers.